Data in Brief 46 (2023) 108826

Contents lists available at ScienceDirect

Data in Brief

journal homepage: www.elsevier.com/locate/dib

Data Article

Mineral chemistry dataset of the Tournaisian – Lower Viséan submarine basaltic volcanism of the Matachel Basin (SW Iberian Massif).

F. Sarrionandia[a,*], J. Errandonea-Martin[b], E. Larrondo[c], M. Carracedo-Sánchez[b], B. Ábalos[b], J.I. Gil-Ibarguchi[b]

[a] *Departamento de Geología, Facultad de Farmacia, Universidad del País Vasco UPV/EHU, 01006 Vitoria-Gasteiz, Spain*
[b] *Departamento de Geología, Facultad de Ciencia y Tecnología, Universidad del País Vasco UPV/EHU, P.O.Box 644, E-48080 Bilbao, Spain*
[c] *Team Ingeniería y Consultoría S.L., Parque Científico y Tecnológico de Bizkaia, 207C, 48170, Zamudio, Spain*

A R T I C L E I N F O

Article history:
Received 21 November 2022
Revised 2 December 2022
Accepted 8 December 2022
Available online 13 December 2022

Dataset link: Mineral chemistry dataset of the Carboniferous submarine basaltic volcanism of the Matachel Basin (SW Iberian Massif) (Original data)

Keywords:
Electron microprobe
Clinopyroxene
Amphibole
Plagioclase
Basalts
Eruption
Carboniferous
Ossa-Morena zone

A B S T R A C T

The Matachel Basin is a tectono-stratigraphic unit of Ossa-Morena Zone (southern Iberian Massif) that encompasses an Upper Tournaisian – Viséan basaltic sequence, generated by effusive and explosive eruptions in a shallow submarine setting. A collection of 23 basaltic and gabbroic samples were selected for detailed petrographic descriptions, which included a mineral chemistry characterization by means of Electron Microprobe analysis in 9 rock samples. In this contribution a total of 501 mineral chemical data are presented, which correspond to plagioclase (208 analysis), clinopyroxene (202 analysis), amphibole (64 analysis), opaque minerals (18 analysis), and alkali feldspar (9 analysis). According to mineral classification diagrams analyzed rock samples are composed by albite-labradorite (An_{01-66}), augite ($Wo_{31-41}En_{32-49}Fs_{7-22}$), magnesiohornblende, ferrohornblende, ferropargasite, titanian magnesiohastingsite, orthoclase (Or_{93-97}), titanomagnetite, and ilmenite. Presented dataset provides a robust information of the nature of the outpouring lava emissions in shallow-marine intra-continental basins, and would enhance a better

* Corresponding author:
E-mail address: fernando.sarrionandia@ehu.eus (F. Sarrionandia).

https://doi.org/10.1016/j.dib.2022.108826

understanding of eruptive dynamics in this type of tectonic settings.

Specifications Table

Subject	Earth and Planetary Sciences
Specific subject area	Geochemistry and Petrology
Type of data	Table Figure
How the data were acquired	Analysis of mineral compositions (major and trace elements) using a CAMECA SX100 Electron Microprobe Microscopic surveys for mineral sample selection were performed with a Leica DM LP device.
Data format	Raw Analyzed
Description of data collection	A collection of 23 basaltic and gabbroic rock samples were selected for detailed petrographic descriptions. After microscopic studies 9 samples with limited hydrothermal alteration were separated for a mineral chemistry characterization by means of Electron Microprobe analysis. Mineral formulas were normalized to 6 oxygen atoms for pyroxene, 23 oxygen atoms for amphibole, 8 oxygen atoms for plagioclase and alkali feldspar, and 4 oxygen atoms for Fe-Ti oxides.
Data source location	University of the Basque Country UPV/EHU, Science and Technology Faculty, SGIker research facility, Leioa (Spain) Samples collected from the 'basic volcanism' unit of the Matachel Basin (Southern Iberian Massif), Badajoz province (SW Spain). See UTM coordinates below.
Data accessibility	Repository name: Mendeley Data Data identification number: doi: 10.17632/dfkkjzb6cw.2 Direct URL to data: https://data.mendeley.com/datasets/dfkkjzb6cw/2

Sample	X	Y	Datum
MGA-2	251773	4251752	ED_50_30N
MGA-20	752977	4267620	ED_50_29N
MGA-22	245772	4255195	ED_50_30N
MTC-48	748736	4271284	ED_50_29N
MTC-75	477760	4254207	ED_50_30N
MTC-83	261375	4248639	ED_50_30N
MTC-274	240985	4259203	ED_50_30N
VFB-9	249958	4252350	ED_50_30N
VFB-12	248639	4252945	ED_50_30N

Value of the Data

- The data provide chemical information to characterize and classify the primary rock-forming minerals of the Carboniferous basic volcanism of the Matachel Basin (SW Iberian Massif; Spain).
- The data can benefit contributions dealing with subaqueous basaltic eruptions.
- The data, with additional information, can gain further insights regarding the Carboniferous volcanism related with the Variscan orogeny and Pangea assembly.

1. Objective

The Southern Iberian Massif records a voluminous Early Carboniferous igneous activity developed in relation with the diachronic oblique collision of Laurussia and Gondwana and the

subsequent structuration of the European Variscan Belt (e.g. [1,2]). This magmatic activity is particularly well represented by intrusive bodies (e.g. [3–5]). Nevertheless, the characteristics of associated volcanic eruptions is still poorly known. The Matachel Basin is a tectono-stratigraphic unit of the southern Iberian Massif which encloses an Upper Tournaisian – Viséan volcano-sedimentary assemblage generated in an intra-continental shallow marine basin [6]. Volcanic outpourings constituted a small lava field, in three distinct volcanic events designed as (from the ancient to the newest): 1) 'acid volcanism I', 2) 'basic volcanism', and 3) 'acid volcanism II' [7]. This contribution presents for the first time the compositional characteristics of the primary mineralogy of the lava deposits and associated shallow subvolcanic intrusions of the 'basic volcanism', essentially represented by basalts and basaltic andesites. Mineral chemistry data here presented provide a robust characterization of the geochemical nature of erupting lavas, enhancing a future better understanding of subaqueous eruptive dynamics in relation with the structuration of the variscan orogen.

2. Data Description

Volcanic deposits generated during the 'basic volcanism' event are integrated by hyalocrystalline to holocrystalline rocks, constituted by variable amounts of devitrified glass, and primary clinopyroxene, plagioclase, and accessory ilmenite and titanomagnetite. This mineral assemblage also constitutes the associated intrusive rocks, besides amphibole, and accessory alkali feldspar, apatite and zircon. Most of studied rocks exhibit a persuasive hydrothermal alteration that has generated a secondary mineral assemblage integrated by sericite, calcite, epidote, chlorite, opaque minerals, sphene, actinolite-tremolite, quartz, biotite, muscovite, and alkali feldspar. Generally, basaltic glass hydration leads to a rather complex glass devitrification process, known as palagonitization, which is normally accompanied by an extensive mobilization of chemical elements (e.g. [8]). In this sense, microscopic surveys of analyzed rocks have shown the absence of fresh glass relicts susceptible of their geochemical characterization. Though overprinted hydrothermal alteration could have remobilized some alkaline and large ion lithophile elements in the studied rocks (e.g. [9]), high field strength elements and some transition elements behave relatively immobile (e.g. [10]), and references therein). Moreover, chemical studies of main rock forming minerals (e.g. olivine and/or pyroxene in ultrabasic-basic igneous rocks) may provide useful information about magma sources, crystallization conditions, and/or post-magmatic processes (e.g. [11–14]). Consequently, chemical composition of the primary crystalline phases can provide some insights about the geochemical characteristics of erupting lavas and associated intrusives. Major- (Si, Ti, Al, Fe, Mn, Mg, Ca, Na, K) and trace-element (Ni, Cr) contents in the preserved primary assemblage (i.e., clinopyroxene, plagioclase, alkali feldspar, amphibole, ilmenite and titanomagnetite) were determined by means of Electron Microprobe analyses. Raw data were deposited to Mendeley Data under the identification number: doi:10.17632/dfkkjzb6cw.2 [15].

Analyzed plagioclases exhibit in general marked compositional variations (Table 1). Plagioclases of both tabular lava-flows and pillow-lava flows are compositionally similar (An_{01-58}), classifying in the compositional fields of albite, oligoclase, andesine and labradorite in the An–Ab–Or diagram (Fig. 1a,b) of [8]. It should be highlighted the near absence of a compositional zonation in these plagioclases (Table 1; Fig. 1a,b). Similarly, compositional characteristics of analyzed plagioclases in gabbroic intrusions are equal to those of volcanic deposits (An_{01-66}), thus overlapping their projection in the same classification fields of the An–Ab–Or diagram (Fig. 1c,d), whereas their compositional range in diorites is markedly narrower (An_{20-39}), classifying as oligoclase and andesine in the An–Ab–Or diagram. It is also remarkable the absence of compositional zonation in the plagioclases of associated intrusive rocks (Table 1; Fig. 1c,d).

Similarly to plagioclase, compositional differences between clinopyroxenes of intrusive rocks ($Wo_{37-41}En_{36-46}Fs_{8-15}$) and extrusive deposits ($Wo_{31-39}En_{32-49}Fs_{7-22}$) are negligible (Table 2), though clinopyroxene of diorites appear completely transformed to ferropargasite. Analyzed clinopyroxene crystals, which lack of compositional zonation, are of Ca–Mg–Fe type [9], clas-

Table 1
Representative feldspar compositions from studied volcanic and plutonic rocks of the 'basic volcanism' of the Matachel Basin (southern Iberian Massif). Raw data available in [15].

	Pl_111	Pl_131	Pl_154	Pl_106	Pl_150	Pl_159	Pl_201	Pl_173	Pl_182	Pl_37	Kfs_3	Kfs_5
Sample	MTC-48	MGA-20	MTC-274	MGA-22	MTC-274	MTC-274	VFB-12	MTC-75	MTC-75	MGA-2	VFB-9	VFB-9
Lithology	Plut.	Plut.	Plut.	Plut.	Plut.	Plut.	Plut.	Volc.	Volc.	Volc.	Volc.	Volc.
Spot	Core	Core	Core	Rim	Rim	Rim	Rim	Core	Core	Rim	-	-
K_2O	0.19	0.17	0.12	0.35	0.06	0.64	0.10	0.16	0.25	0.11	15.74	15.97
CaO	10.88	12.44	7.48	9.75	6.60	4.10	0.19	11.02	8.34	0.52	0.01	0.00
TiO_2	0.14	0.05	0.00	0.05	0.01	0.01	0.03	0.09	0.06	0.00	0.01	0.00
Cr_2O_3	0.03	0.10	0.00	0.00	0.00	0.01	0.02	0.00	0.10	0.04	0.00	0.10
MnO	0.01	0.00	0.00	0.03	0.02	0.01	0.00	0.02	0.00	0.00	0.00	0.00
FeO	0.64	0.59	0.07	0.48	0.24	0.25	0.17	0.71	0.55	0.11	0.14	0.05
NiO	0.00	0.05	0.06	0.06	0.06	0.00	0.00	0.03	0.00	0.00	0.00	0.00
Na_2O	5.38	4.47	7.49	5.90	8.10	8.81	11.24	5.23	6.77	11.52	0.60	0.31
SiO_2	54.49	52.50	59.05	55.85	59.92	62.13	68.46	54.48	57.93	67.87	64.54	64.62
Al_2O_3	27.33	28.59	24.98	26.61	24.41	23.12	19.56	27.38	25.25	19.33	17.83	17.96
MgO	0.09	0.14	0.00	0.06	0.00	0.00	0.01	0.14	0.06	0.03	0.00	0.02
Total	99.19	99.10	99.24	99.14	99.43	99.08	99.77	99.26	99.32	99.53	98.88	99.03
An	0.52	0.60	0.35	0.47	0.31	0.20	0.01	0.53	0.40	0.02	0.00	0.00
Ab	0.47	0.39	0.64	0.51	0.69	0.77	0.99	0.46	0.59	0.97	0.05	0.03
Or	0.01	0.01	0.01	0.02	0.00	0.04	0.01	0.01	0.01	0.01	0.94	0.97

Pl: plagioclase; Kfs: K-feldspar; Plut.: plutonic; Volc.: volcanic; An: anortite; Ab: albite; Or: Othoclase.

Table 2
Representative pyroxene compositions from studied volcanic and plutonic rocks of the 'basic volcanism' of the Matachel Basin (southern Iberian Massif). Raw data available in [15].

	Px_01	Px_18	Px_ 100	Px_16	Px_20	Px_ 104	Px_ 105	Px_28	Px_45	Px_ 197	Px_46	Px_ 199
Sample	MTC-83	MTC-83	MTC-48	MTC-83	MTC-83	MTC-48	MTC-48	MGA-2	MGA-2	VFB-9	MGA-2	VFB-9
Lithology	Plut.	Plut.	Plut.	Plut.	Plut.	Plut.	Plut.	Volc.	Volc.	Volc.	Volc.	Volc.
Spot	Core	Core	Core	Rim	Rim	Rim	Rim	Core	Core	Core	Rim	Rim
SiO_2	49.75	51.36	51.38	49.79	50.90	50.24	50.89	51.44	49.37	52.85	51.84	53.06
TiO_2	1.61	1.04	0.85	1.62	1.21	1.18	1.00	0.75	1.35	0.70	0.73	0.67
Al_2O_3	2.85	2.09	1.53	3.29	1.96	2.49	3.05	1.60	3.60	1.88	1.54	2.00
FeO	10.12	7.83	10.18	8.53	9.15	10.61	6.70	12.53	10.94	6.68	12.76	6.59
Cr_2O_3	0.00	0.00	0.03	0.00	0.05	0.05	0.46	0.00	0.08	0.04	0.00	0.04
NiO	0.00	0.00	0.00	0.00	0.00	0.07	0.06	0.08	0.00	0.05	0.03	0.00
MnO	0.29	0.17	0.31	0.22	0.21	0.28	0.15	0.39	0.34	0.20	0.40	0.13
MgO	12.98	14.81	14.64	13.82	14.01	13.61	15.52	15.37	13.17	16.92	15.45	16.87
CaO	21.17	21.56	20.08	21.33	21.44	20.31	21.15	16.97	19.99	21.35	16.52	20.74
Na_2O	0.50	0.39	0.30	0.45	0.44	0.39	0.29	0.27	0.47	0.32	0.30	0.25
K_2O	0.02	0.01	0.01	0.00	0.01	0.00	0.00	0.00	0.01	0.00	0.00	0.01
Total	99.28	99.25	99.31	99.06	99.37	99.23	99.28	99.41	99.32	100.98	99.57	100.36
Woll	0.40	0.40	0.37	0.38	0.41	0.37	0.38	0.32	0.35	0.38	0.31	0.39
En	0.36	0.41	0.41	0.39	0.39	0.38	0.43	0.43	0.37	0.46	0.43	0.46
Fs	0.13	0.10	0.14	0.11	0.12	0.14	0.09	0.18	0.14	0.07	0.20	0.10
mg#	0.75	0.80	0.75	0.79	0.77	0.74	0.84	0.71	0.73	0.87	0.69	0.83

Px: pyroxene; Plut.: plutonic; Volc.: volcanic; Woll: wollastonite; En: enstatite; Fs: ferrosilite.

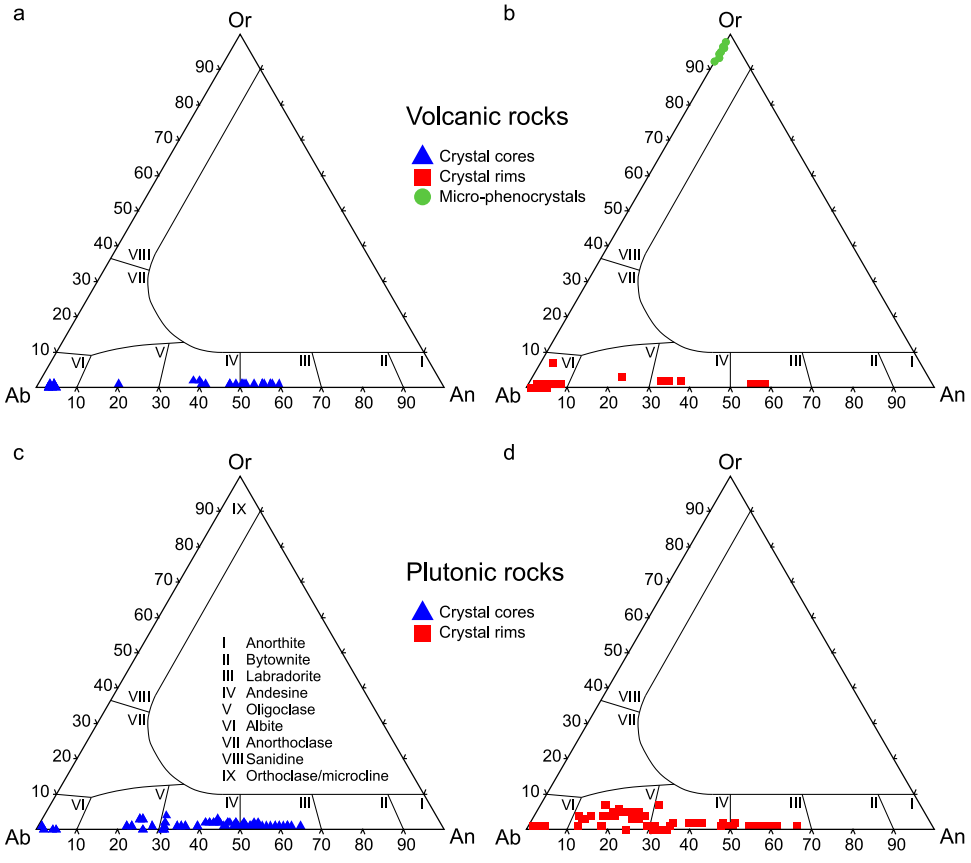

Fig. 1. Projection of analysed feldspars of the 'basic volcanism' of the Matachel Basin (southern Iberian Massif) in the An–Ab–Or clinopyroxenes classification diagram of [16]. a) plagioclase cores, and b) feldspars rims of analysed volcanic rocks. c) plagioclase cores, and d) plagioclase rims of analysed plutonic rocks.

sifying as augites in the Wo–En–Fs diagram (Fig. 2). These augites exhibit relatively high Mg# values (lava-flows: 0.61–0.88; gabbros: 0.71–0.85), and marked variations in Cr_2O_3 (0–0.72 wt.%) and TiO_2 (0.47–3.54 wt.%) contents (Table 2).

Amphibole appears restricted to intrusive rocks, constituting coronitic textures with, or replacing partially or totally, clinopyroxene crystals. According to the amphibole classification diagram of [10], in the gabbros isolated single crystals of this mineral correspond with actinolite and magnesiohornblende, whereas amphibole replacing clinopyroxene are classified as titanian magnesiohastingsite (Fig. 3; Table 3). Amphiboles in gabbros lack compositional variations, being characterized by their low Cr contents (< 0.03 apfu). Analyzed actinolite and magnesiohornblende are characterized by low Ti contents (0.03–0.13 apfu) and relatively high $Mg/(Mg+Fe^{2+})$ ratios (0.58–0.73), with wide ranges in the cation site occupancies in $(Na+K)^{A}$ (0.07–0.32 apfu) and Al^{IV} (0.35–0.71 apfu) (Table 3). Contrarily, titanian magnesiohastingsite exhibits high Ti contents (0.32–0.40 apfu) and relatively narrow $Mg/(Mg+Fe^{2+})$ ratios (0.60–0.69). Similarly cation site occupancies are relatively homogeneous for $(Na+K)^{A}$ (0.63–0.74 apfu) and Al^{IV} (1.48–1.78 apfu) (Table 3).

In the diorites isolated amphibole crystals classify as magnesiohornblende and ferrohornblende, whereas amphiboles replacing clinopyroxene are classified as ferropargasite (Fig. 3;

Table 3
Representative amphibole compositions from studied volcanic and plutonic rocks of the 'basic volcanism' of the Matachel Basin (southern Iberian Massif). Raw data available in [15].

	Amp_24	Amp_18	Amp_08	Amp_14	Amp_03	Amp_60	Amp_30	Amp_34	Amp_32	Amp_59	Amp_62	Amp_51
Sample	MTC-274	MTC-274	MGA-22	MGA-22	MGA-22	MTC-274	MGA-22	MGA-22	MGA-22	MTC-274	MTC-274	MTC-274
Lithology	Plut.	Plut.	Plut.	Plut.	Plut.	Plut.	Plut.	Plut.	Plut.	Plut.	Plut.	Plut.
Spot	Rim	Core	Rim	Core	Rim	Core	Core	Rim	Rim	Core	Core	Core
SiO_2	39.89	40.67	42.27	41.89	43.24	42.71	51.92	53.01	50.90	46.33	46.02	44.15
TiO_2	0.32	0.44	3.01	3.54	2.80	2.22	0.30	0.39	0.79	1.51	1.26	1.81
Al_2O_3	14.64	14.05	9.58	10.27	8.68	8.97	2.77	2.56	3.42	6.63	7.65	9.52
Cr_2O_3	0.00	0.01	0.08	0.00	0.00	0.00	0.00	0.04	0.00	0.05	0.03	0.00
FeO	20.20	20.04	15.28	13.60	16.35	19.53	17.09	12.37	14.30	18.78	17.96	17.57
MgO	6.54	7.10	11.89	12.68	11.47	8.60	12.80	16.49	14.77	10.05	10.36	9.57
MnO	0.22	0.32	0.26	0.19	0.24	0.40	0.35	0.25	0.26	0.35	0.26	0.27
CaO	11.59	11.46	10.83	11.06	10.78	10.88	11.64	10.87	10.82	11.03	11.51	11.51
Na_2O	1.70	1.49	2.38	2.63	2.43	1.66	0.40	0.65	1.07	1.32	1.24	1.46
K_2O	1.12	1.02	0.97	0.75	0.85	0.78	0.10	0.20	0.24	0.56	0.55	0.85
Total	96.27	96.61	96.54	96.60	96.91	95.85	97.36	96.93	96.58	96.62	96.87	96.69
Si	6.15	6.21	6.37	6.26	6.52	6.58	7.64	7.64	7.46	6.99	6.90	6.67
Ca_B	1.91	1.87	1.75	1.77	1.74	1.80	1.84	1.68	1.70	1.78	1.85	1.86
$(Na+K)_A$	0.64	0.52	0.68	0.69	0.66	0.46	0.07	0.11	0.20	0.29	0.32	0.45
Ti	0.04	0.05	0.34	0.40	0.32	0.26	0.03	0.04	0.09	0.17	0.14	0.21
Al^{VI}	0.81	0.74	0.07	0.07	0.06	0.21	0.12	0.08	0.05	0.17	0.26	0.37
Fe^{3+}	0.44	0.56	0.40	0.39	0.33	0.42	0.16	0.20	0.28	0.41	0.37	0.28
mg#	0.41	0.45	0.64	0.68	0.60	0.48	0.59	0.73	0.69	0.54	0.55	0.53
	Fprg	Fprg	Mhs	Mhs	Ed	Fhb	Act	Act	Mhb	Mhb	Mhb	Mhb

Amp: amphibole; Plut.: plutonic; Volc.: volcanic; Fprg: ferropargasite; Mhs: magnesiohastingsite; Ed: Edenite; Fhb: ferrohornblende; Act: actinolite; Mhb: magnesiohornblende.

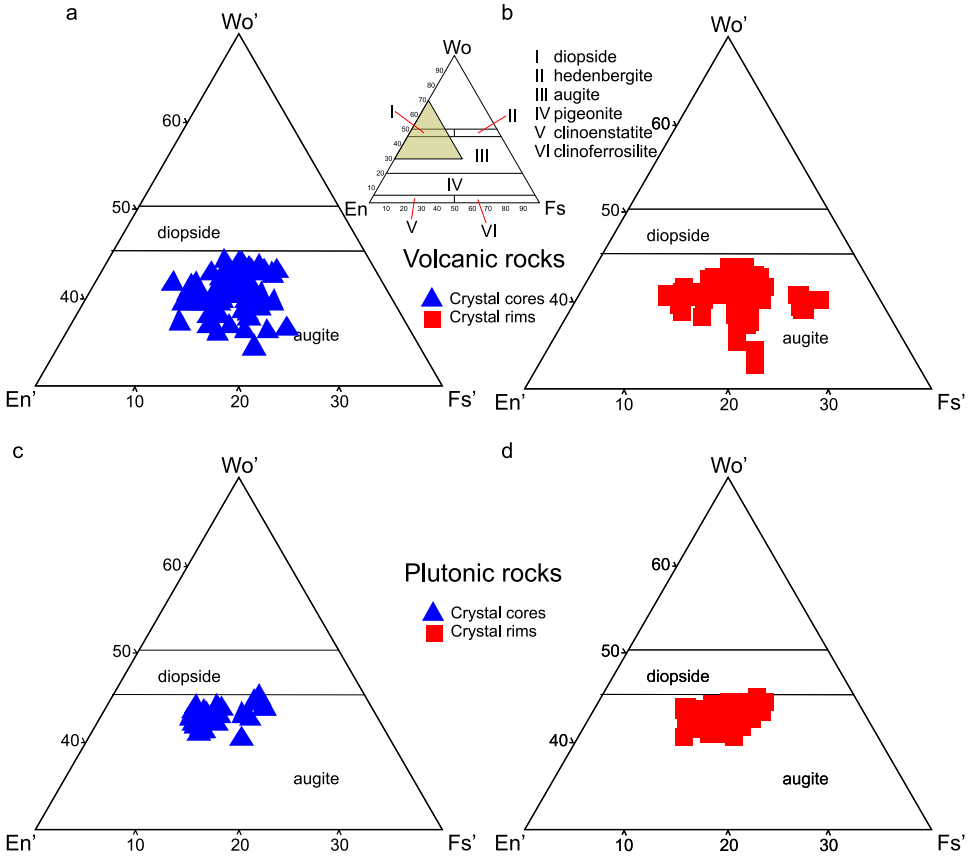

Fig. 2. Projection of analysed pyroxenes of the 'basic volcanism' of the Matachel Basin (southern Iberian Massif) in the Ca–Mg–Fe clinopyroxenes classification diagram of [17]. a) pyroxene cores, and b) pyroxene rims of analysed volcanic rocks. c) pyroxene cores, and d) pyroxene rims of analysed plutonic rocks.

Table 3). These amphiboles are also characterized by their markedly low Cr contents (< 0.01 apfu) and the absence of compositional zonations (Table 3). Magnesiohornblende and ferrohornblende exhibit higher cation site occupancies in $(Na+K)^{A}$ (0.21–0.46 apfu), Al^{IV} (1.01–1.42 apfu), and Ti (0.08–0.26 apfu), respect to those amphiboles found in studied gabbros (Table 3). But their $Mg/(Mg+Fe^{2+})$ ratios (0.48–0.60) are only slightly lower (Table 3). Ferropargasites are characterized by their lower Ti contents (0.04–0.09 apfu) and $Mg/(Mg+Fe^{2+})$ ratios (0.41–0.48), with a wider range in the cation site occupancies in $(Na+K)^{A}$ (0.50–0.64 apfu) and Al^{IV} (1.67–1.89 apfu) than those of analyzed titanian magnesiohastingsite (Table 3).

Analyzed opaque minerals correspond with titanomagnetite and ilmenite (Table 4). Finally, alkali feldspar has only been detected in a pillow-lava flow (sample VFB-9), where appears as an interstitial phase in the mesostasis. This accessory mineral is classified as orthoclase (Or_{93-97}) in the classification diagram for feldspars of [8] (Table 1; Fig. 1a,b).

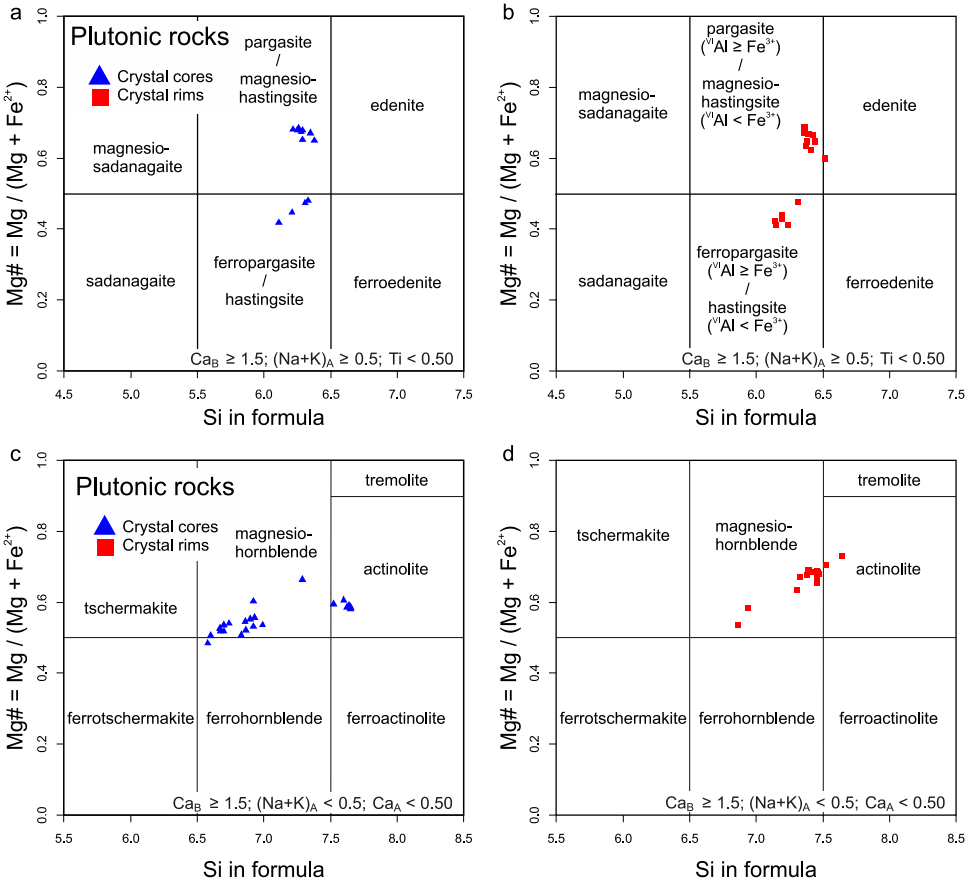

Fig. 3. Projection of analysed amphiboles of the 'basic volcanism' of the Matachel Basin (southern Iberian Massif) in the classification diagram for calcic amphiboles of [18]. a and b) Calcic amphiboles with $(Na+K)_A \geq 0.5$. c and d) Calcic amphiboles with $(Na+K)_A < 0.5$.

Table 4
Representative ilmenite and magnetite compositions from studied volcanic and plutonic rocks of the 'basic volcanism' of the Matachel Basin (southern Iberian Massif). Raw data available in [15].

	Ilm_1	Ilm_4	Ilm_7	Ilm_9	Mag_1	Mag_2	Mag_4	Mag_5	Mag_6	Mag_8
Sample	MGA-20	MTC-48	MGA-2	VFB-9	MGA-20	MGA-20	MTC-48	MGA-2	MGA-2	MGA-2
Lithology	Plut.	Plut.	Volc.	Volc.	Plut.	Plut.	Plut.	Volc.	Volc.	Volc.
SiO_2	0.08	0.04	0.08	0.04	0.15	0.08	0.12	0.13	0.08	0.08
TiO_2	45.80	50.97	45.81	51.22	0.99	7.41	12.26	1.04	7.41	12.26
NiO	0.00	0.10	0.00	0.08	0.05	0.00	0.00	0.05	0.00	0.00
Al_2O_3	0.53	0.03	0.06	0.01	0.72	0.31	2.87	0.66	0.29	2.69
Cr_2O_3	0.05	0.00	0.00	0.04	0.05	0.05	0.52	0.05	0.04	0.51
FeO	50.53	42.57	50.06	41.72	92.20	87.15	72.98	91.98	86.08	71.85
MgO	0.13	0.00	0.13	0.00	0.05	0.01	0.08	0.01	0.02	0.06
MnO	2.24	5.46	2.34	6.04	0.00	0.31	2.22	0.00	0.41	2.00
CaO	0.05	0.19	0.05	0.07	0.06	0.01	0.06	0.06	0.01	0.06
Na_2O	0.00	0.01	0.00	0.01	0.00	0.00	0.03	0.00	0.00	0.04
K_2O	0.00	0.00	0.00	0.00	0.00	0.00	0.00	0.00	0.00	0.00
Total	99.41	99.37	98.55	99.23	94.27	95.34	91.13	93.98	94.34	89.54
Fe^{3+}	0.00	0.00	0.00	0.00	1.90	1.56	1.12	1.90	1.55	1.11
Fe^{2+}	1.59	1.35	1.60	1.33	1.03	1.20	1.28	1.03	1.20	1.29

Ilm: ilmenite; Mag: magnetite; Plut.: plutonic; Volc.: volcanic

3. Experimental Design, Materials and Methods

Hand samples were inspected to the naked eye, magnifying glasses and trinocular stereomicroscope, then cut with a diamond blade saw by technical staff of the rock sample preparation service at the University of the Basque Country UPV/EHU (Leioa, Spain). Petrographic thin sections (30 μm thick) from rock samples cuttings were prepared by personnel from the aforementioned facility. The glass slide preparation dimensions were 48 mm long and 28 mm short. For the microscopic study of thin sections, a Leica DMLP polarizing microscope was used, equipped with transmitted and reflected light, and digital camera (Nikon DS-Fi1). Mineral analyses (accessible in [15]) were performed on polished, carbon coated thin sections by electron microprobe methods (EMPA) using a Cameca SX-100 instrument equipped with a Energy Dispersive (EDS) and five Wavelength Dispersive (WDS) spectrometers at the University of Oviedo (Oviedo, Spain). Operating conditions of the microprobe were: 5 μm beam diameter, 10 s counting time (peak), $\sim$10 nA beam current intensity and 15 kV accelerating voltage. Calibration was done against French Geological Survey (BRGM) standard minerals and the PAP matrix correction model was used. Structural formulae of minerals and graphical projection of mineral compositions were carried out using an unpublished R-language plugin for the *GCDkit* software of [19].

Ethics Statements

Presented data do not involve human subjects, animal experiments, or any data collected from social media platforms, and follow the ethical requirements of the Data in Brief.

CRediT Author Statement

Fernando Sarrionandia: Investigation, Data Curation, Visualization, Writing - Original draft; **Jon Errandonea-Martin**: Formal analysis, Data curation, Visualization; **Egoitz Larrondo**: Inves-

tigation, Resources; **Manuel Carracedo-Sánchez:** Investigation, Resources, Supervision; **Benito Ábalos**: Writing – Reviewing and Editing; **José Ignacio Gil Ibarguchi:** Writing – Reviewing and Editing, Project administration.

Declaration of Competing Interest

The authors declare that they have no known competing financial interests or personal relationships that could have appeared to influence the work reported in this paper.

Data Availability

Mineral chemistry dataset of the Carboniferous submarine basaltic volcanism of the Matachel Basin (SW Iberian Massif) (Original data) (Mendeley Data).

Acknowledgments

Financial support was provided by the Basque Country University UPV/EHU (Project GIU20/10). Technical and human support provided by the Scientific and Technical Services facilities (Oviedo University, MAF) is acknowledged.

References

[1] M.F. Pereira, M. Chichorro, S.T. Johnston, G. Gutiérrez-Alonso, J.B. Silva, U. Linnemann, K. Drost, The missing Rheic Ocean magmatic arcs: provenance analysis of Late Paleozoic sedimentary clastic rocks of SW Iberia, Gondwana Res. 22 (2012) 882–891, doi:10.1016/j.gr.2012.03.010.
[2] M.F. Pereira, G. Gutiérrez-Alonso, J.B. Murphy, K. Drost, C. Gama, J.B. Silva, Birth and demise of the Rheic Ocean magmatic arc(s): combined U–Pb and Hf isotope analyses in detrital zircon from SW Iberia siliciclastic strata, Lithos 278 (2017) 383–389, doi:10.1016/j.lithos.2017.02.009.
[3] J. Pons, in: Ph.D. thesis, University of Toulouse, 1982, p. 451.
[4] F. Sarrionandia, M. Carracedo, L. Eguíluz, J. Junguitu, P. Lobo, J.I. Gil Ibarguchi, Geologic map of the Valencia del Ventoso Variscan igneous complex (SW Iberian Massif, Spain): An example of multi-stage intrusion building by contrasted magma compositions, J. Map. 9 (4) (2013) 498–504, doi:10.1080/17445647.2013.820675.
[5] J. Errandonea-Martin, F. Sarrionandia, V. Janoušek, M. Carracedo-Sánchez, J.I. Gil Ibarguchi, Origin of cordierite-bearing monzogranites from the southern Central Iberian Zone – Inferences from the zoned Sierra Bermeja Pluton (Extremadura, Spain), Lithos 342–343 (2019) 440–462, doi:10.1016/j.lithos.2019.06.009.
[6] V. Gabaldón, A. Garrote, C. Quesada, Geología del Carbonífero inferior del Norte de la Zona de Ossa Morena. Introducción a la excursión, in: V Reunión del Grupo de Ossa Morena, Bélmez (Córdoba), Temas Geológicos-Mineros 7, IGME, , Madrid, 1985, pp. 101–137.
[7] O. Apalategui, P. Higueras, C. Quesada, Mapa Geológico de España a E. 1:50.000 n° 855 (Usagre), 2°serie-MAGNA, ed.,, IGME, Madrid, 1983.
[8] N.A. Stroncik, H.U. Schmincke, Palagonite – a review, Int. J. Earth Sci. 91 (4) (2002) 680–697, doi:10.1007/s00531-001-0238-7.
[9] S.E. Humphries, The mobility of the rare earth elements in the crust, in: P. Henderson (Ed.), Rare Earth Element Geochemistry, Elsevier, Amsterdam, 1984, pp. 315–341.
[10] C. Pin, J. Waldhausrová, Sm-Nd isotope and trace element study of Late Proterozoic metabasalts ("spilites") from the Central Barrandian domain (Bohemian Massif, Czech Republic), in: U. Linnemann, R.D. Nance, P. Kraft, G. Zulauf (Eds.), The Evolu- tion of the Rheic Ocean: From Avalonian-Cadomian Active Margin to Alleghenian- Variscan Collision, Geological Society of America, Boulder, 2007, pp. 231–247, doi:10.1130/2007.2423(10). Special Paper 423.
[11] T. Gasparik, Two-pyroxene thermobarometry with new experimental data in the system CaO-MgO-Al2O3-SiO2, Contr. Mineral. Petrol. 87 (1984) 87–97, doi:10.1007/BF00371405.
[12] G. Witt-Eickschen, U. Kramm, Mantle upwelling and metasomatism beneath Central Europe: geochemical and isotopic constraints from mantle Xenoliths from the Rhön (Germany), J. Petrol. 38 (4) (1997) 479–493, doi:10.1093/petroj/38.4.479.
[13] J. Sun, C.-Z. Liu, F.-Y. Wu, Y.-H. Yang, Z.-Y. Chu, Metasomatic origin of clinopyroxene in Archean mantle xenoliths from Hebi, North China Craton: Trace-element and Sr-isotope constraints, Chem. Geol. 328 (2012) 23–136, doi:10.1016/j.chemgeo.2012.03.014.
[14] G. Cao, Y. Tong, X. Li, L. Wang, Insights from olivine chemistry into crustal magmatic processes and the mantle source lithology of basalts from Hainan Island, China, Lithos 430–431 (2022) 106852, doi:10.1016/j.lithos.2022.106852.

[15] F. Sarrionandia-Ibarra, Mineral chemistry dataset of the Carboniferous submarine basaltic volcanism of the Matachel Basin (SW Iberian Massif), Mendeley Data 2 (2022) v https://data.mendeley.com/datasets/dfkkjzb6cw/2 .
[16] W.A. Deer, R.A. Howie, J. Zussman, Rock-Forming Minerals, vol. 4, Framework Silicates, ed, Longman, London, 1963.
[17] N. Morimoto, Nomenclature of Pyroxenes, Mineral. Petrol. 39 (1) (1988) 55–76, doi:10.1007/BF01226262.
[18] B.E. Leake, A.R. Woolley, C.E.S. Arps, W.D. Birch, M.C. Gilbert, J.D. Grice, F.C. Hawthorne, A. Kato, H.J. Kisch, V.G. Krivovichev, K. Linthout, J. Laird, J.A. Mandarino, W.V. Maresch, E.H. Nickel, N.M.S. Rock, J.C. Schumacher, D.C. Smith, N.C.N. Stephenson, L. Ungaretti, E.J.W. Whittaker, G. Youzhi, Nomenclature of amphiboles. Report of the Subcommittee on Amphiboles of the International Mineralogical Association, Commission on the New Mineral Names, Can. Mineral 35 (1997) 219–246.
[19] V. Janoušek, C.M. Farrow, V. Erban, Interpretation of whole-rock geochemical data in igneous geochemistry: introducing geochemical data toolkit (GCDkit), J. Petrol. 47 (6) (2006) 1255–1259, doi:10.1093/petrology/egl013.